Strain localization in geomaterials and regularization: rate-dependency, higher order continuum theories and multi-physics

Ioannis Stefanou[1] **and Eleni Gerolymatou**[2]

[1] *Université Paris-Est, Laboratoire Navier, CNRS UMR 8205, IFSTTAR, ENPC, France*
[2] *Chalmers University of Technology, Sweden*

Strain localization is a central topic in geomechanics as it is often related to failure and other important physical phenomena and geological processes.
This chapter is addressed to graduate students and researchers interested in an introduction to strain localization analysis. We present fundamental notions that are frequently met in this topic, such as loss of uniqueness, bifurcation, stability, ill-posedness and mesh-size dependency.
We first show the inherent pathology of classical, Cauchy, rate-independent continua that leads to mesh sensitivity and we present methods for alleviating/regularizing this problem. These methods involve the use of theories that result in the introduction of characteristic time and length scales into the system. We focus mainly on rate-dependent constitutive laws, Micromorphic continua and multiphysics.
Regularization of strain localization is shown as general as possible using bifurcation and stability analysis and without prescribing exact constitutive relations. One-dimensional examples are then used to illustrate each regularization approach and show in a mathematically simple manner the main results.

1 Introduction

Strain localization is an important phenomenon in geomechanics. From a geometrical point of view, strain localization is related to the creation of (quasi-)periodic geometrical patterns as in figure 1. From an engineering point of view strain localization is related to failure. For instance, failure of a retaining wall happens through the localization of strain at the slip surface. At a larger scale, landslides or even earthquakes

Figure 1: Network of quasi-periodic compaction bands (see paragraph 2.3 for definition) at Valley of Fire, Nevada, USA (date of photo: 25/12/2015).

occur due to localized, intense shear deformation in a narrow zone of millimetric to centimetric scale.

In this chapter we give the fundamental tools for studying a) the conditions for which strain localization takes place and b) its type. We focus mainly on deformation bands, which are frequently observed in nature and in engineering applications. However, the methodology that is developed can be applied for more complex patterns of strain localization as is for example the checkerboard pattern shown in figure 2, diffusion and/or run-away modes (e.g. [VS95, ND11, BSS17]).

The methodology we follow is based on bifurcation and stability theory of dynamical systems. This theory gives a unified, general and rigorous mathematical framework for studying strain localization in solids. It is worth emphasizing that, despite the various theoretical and mathematical complications related to constitutive modeling and multiphysics couplings (see [LCBD09, Bow09] for some good references in continuum mechanics and constitutive modeling), once the equations for the (dynamical) system are established, bifurcation (and stability) analysis is a standard methodology.

In Section 2 we give the necessary definitions of common terms that are often found in the literature when studying strain localization. We explain what is loss of uniqueness, bifurcation, stability, ill-posedness and mesh-size dependency and we emphasize their differences. We then focus on deformation bands, their various types and we discuss the necessary conditions for their triggering (onset of localization). Next we

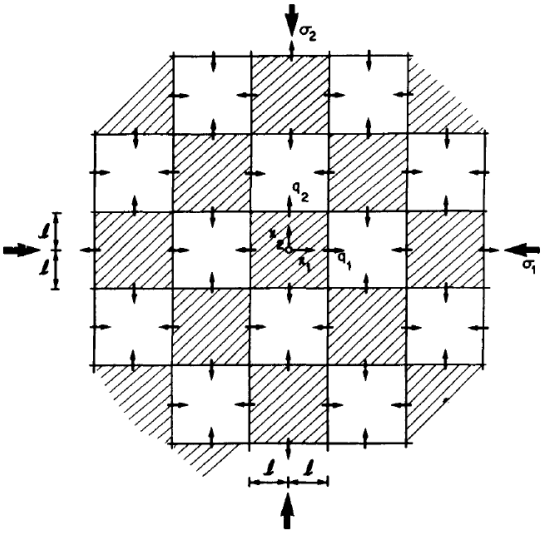

Figure 2: Checkerboard pattern of dilating and contacting cells in water-saturated granular medium (source: [VS95])

.

use the first Lyapunov method in order to derive qualitative estimations regarding the thickness of the deformation band and its evolution. Furthermore, we explain why in rate-independent Cauchy continua strain localization occurs on a mathematical plane (deformation band of zero thickness), which is a mathematical and physical artifact when experimental evidence is taken into account. As a consequence we show why mesh dependency takes place when the finite element method is used for solving strain localization problems.

In order to overcome the aforementioned mathematical and numerical artifacts several approaches have been proposed in the literature for *regularization*. Here we explore the following three regularization techniques. First, we present rate-dependent Cauchy continua (Section 3), their ability to regularize the problem and their limitations. Scale analysis is performed showing the characteristic time scale that rate-dependent Cauchy materials introduce to the strain localization problem. In this way we highlight the physics and the interplay of viscous, inertia and rate-independent terms and we show when each one of them is dominant. Second, in Section 4, we show the general class of Micromorphic continua (e.g. strain gradient theory and Cosserat continuum [Ger73b, Ger73a, CCM01, Var09]), which regularize the problem by introducing characteristic lengths. Finally, going a step further from a pure mechanical description, we show in Section 5 the effect of multiphysics couplings that insert both characteristic lengths and time scales in the problem [Var96a, Var96b, Ben05]. It is needless to say that the literature in each one of this topics is huge and can be classified material-wise, application-wise and method-wise.

Here we use simple one-dimensional examples in order to present the mathematical developments in a simplified manner and to help understanding. These examples follow after a general presentation of the regularization techniques in three-dimensions. Index notation is used throughout this chapter as it is easier for handling the simple case of Cauchy continua and of Micromorphic continua with or without multiphysics couplings.

This chapter is addressed to graduate students and researchers interested in strain localization analysis and can be read in any order. Readers that want a synthesis of the different regularization techniques are advised to follow the order of the sections. Readers that prefer a *"hands-on approach"* are advised to start from the 1D examples in each section and repeat the calculations.
After studying this chapter we hope that the you will be able to:

- Understand fundamental notions related to bifurcation theory;
- Perform a bifurcation analysis using the first Lyapunov method and derive the conditions for strain localization under different constitutive assumptions and continua;
- Identify the dominant time and spatial scales in a class of problems;
- Draw qualitative conclusions regarding strain localization zone thickness and mesh-size dependency without cumbersome numerical analyses;
- Understand the added-value of Micromorphic continua such as the Cosserat and strain-gradient continua;
- Investigate the effect of multiphysics couplings on the localization of deformations.

Updated versions of this chapter can be found at: `http://coquake.eu/index.php/tools/alert_2019/`.

2 Strain localization

Strain localization is a phenomenon that is frequently met in (geo-)materials when strain is localized into narrow zones of increased deformation. Instability, loss of uniqueness, bifurcation, ill-posedness and mesh-size dependency are terms that are frequently used in the literature (some times erroneously or as unwitting abuse of language) to describe this phenomenon from a mathematical point of view. Before studying strain localization in details and proposing various regularization strategies, it is worth define the meaning of each term.

2.1 Definitions

Loss of uniqueness, *bifurcation* and (*in*)*stability* are distinct, but related notions that are frequently used to describe the behavior of physical systems.

Loss of uniqueness and bifurcation are associated with the existence of one or several equilibrium states of a system. These equilibrium states are also called *steady-states* can be periodic in time or time-independent. Of course, the system has to be non-linear in order to have several equilibria and not just only one. They can depend also on several parameters whose value can determine the existence and the number of this equilibrium states. In this case, these parameters are called *bifurcation parameters*. Examples of bifurcation parameters is the loading intensity, the constitutive parameters of a material, geometry etc.

Besides the existence of one or several steady states for given values of the bifurcation parameters, an equilibrium state may be *stable* or *unstable*. We say that an equilibrium (or steady state) is stable when it returns or stays close to this equilibrium after a small perturbation. An equilibrium is unstable when it is not stable. The notion of stability is well established and mathematically rigorously defined in the original work of Lyapunov [Lya92] in the end of 19^{th} century. Stability is directly connected with the *time evolution* of a system. This is in important point, because even if in common practice time is neglected (e.g. quasi-static conditions), the transition from a steady-state to another one happens in a certain time scale, which might be very short (sudden failure of a brittle material) or very slow (geological phenomena).

According to the above, stability and bifurcation (or loss of uniqueness) are two different notions. However, bifurcation points are commonly accompanied with stability change of the equilibrium states. This is illustrated in the following example. In figure 3 we present a simple mechanical system consisted of a rigid bar attached to a pivot point and a spring, and loaded with a load P. We choose the applied load P as bifurcation parameter and we plot the angle θ at equilibrium as a function of P. The space (θ^*, P^*) is called (bifurcation) parameter space and the asterisk denotes equilibrium. Solid lines denote stable equilibrium states and dashed unstable ones. Obviously this system has several equilibria. For instance, for $P^* < -kl$, where l is the length of the bar, the system has two equilibrium states. The first one is when the bar is at vertical upward position $\theta^* = 0$ and it is stable. The second one is when the bar is vertical but downwards ($\theta^* = \pi$) and it is unstable. When $-kl < P^* < kl$ the system has three equilibrium positions, but all are unstable except the one corresponding to $\theta* = 0$. In this system there is no unique equilibrium and therefore the term loss of uniqueness is of no use. However, if one linearizes the system in the vicinity of the $\theta = 0$, then the equilibrium branch for $\theta^* = \pi$ disappears. In this case (see figure 3) the system has a unique equilibrium point for $\theta^* = 0$, which is lost at $P^* = kl$ (loss of uniqueness at the bifurcation point B). For rigorous mathematical definitions of bifurcation, loss of uniqueness and stability we refer to [Lya92, BN69, CCV04, BH91b, BH91a, SA16]. Another, important term that is common in the study of physical systems is *ill-posedness*. A mathematical system is

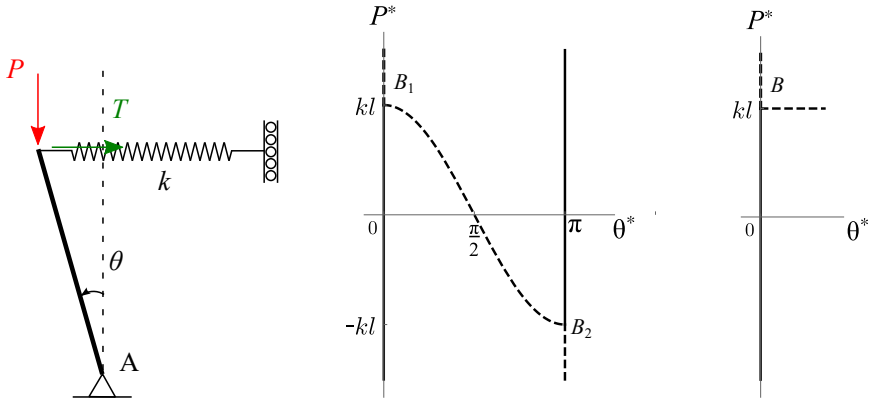

Figure 3: Left: Spring-rigid bar mechanical system. Middle: Bifurcation diagram of the spring-rigid bar system. B_1 and B_2 are bifurcation points. Right: Bifurcation diagram of the linearized spring-rigid bar system in vicinity of $\theta = 0$. The linearized system has only one bifurcation point, B. Solid lines denote stable equilibrium and dashed unstable ones.

said to be *well-posed* when:

- A solution exists;
- The solution is unique;
- The solution's behavior changes continuously with the initial conditions.

This definition is given by Hadamard [Had02]. Problems that are not well-posed in the sense of Hadamard are termed ill-posed. Hadamard believed that problems that are physically important are both solvable and uniquely solvable. However, nowadays we know that the many among the most important modern problems are not uniquely solvable. Examples of very important ill-posed problems are found in all scientific disciplines. Strain localization, inverse problems (e.g. seismic inversion), earthquake nucleation, neural networks, population growth, weather and chaos are some problems involving ill-posed mathematical equations among many others. Even the very simple example given in figure 3 is ill-posed in the sense of Hadamard as multiple equilibria (solutions) exist.

Ill-posed problems are though difficult to solve and these difficulties appear in different forms depending on the application. For example, strain localization is connected with mesh dependency in finite elements analyses. Mesh-size dependency means that the stress-strain response of the system, as well as the strain localization thickness (when interested in deformation bands, see below) depend on the size of the finite element discretization used for solving the problem and further refinement of the mesh does not assure convergence to a unique solution. In order to remedy mesh-size dependency and other undesired and nonphysical phenomena that are frequently met in

ill-posed problems, *regularization* is needed.

A mathematical problem is regularized either ad-hoc by changing the mathematical equations to alleviate undesired pathologies or by introducing more physics to the problem at hand. The mathematical problem might still remain ill-posed, but it will be free of nonphysical behaviors which are not confirmed by observations. Such an example is the formation of shear bands in rate-independent granular materials. As it will be shown below, modeling with the classical Cauchy continuum leads to the formation of shear bands of zero thickness, which is contrary to experimental evidence. Experiments show (e.g. [AHV$^+$12]) that the shear band thickness is finite and equal to some grain particles in size. Mühlhaus and Vardoulakis [MV87] regularized this problem by introducing the missing integral lengths in the mathematical problem by resorting to Cosserat theory (see section 4).

2.2 Instability of homogeneous deformation

The general PDEs of the problem are:

$$\sigma_{ij,j} = \rho \ddot{u}_i, \tag{1}$$

where σ_{ij} is the Cauchy stress tensor, ρ is the density of the material, u_i represents the displacement at direction "i" and the double dot denotes the second time derivative (acceleration). The indices take values $1, 2, 3$ and Einstein summation convention is used herein. Suppose a homogeneous, homogeneously deformed solid that is in equilibrium:

$$\sigma^*_{ij,j} = 0. \tag{2}$$

We assume a perturbation, $\tilde{u}_i$ from the reference, homogeneous solution, u^*_i, such that $\tilde{u}_i = u_i - u^*_i$. $\tilde{u}_i = 0$ at the part of the boundary where displacements are applied and $\tilde{u}_{i,j} n_j = 0$ where tractions are applied. We consider the class of materials whose constitutive law can be written (linearized) as follows:

$$\tilde{\sigma}_{ij} = L_{ijkl} \tilde{\varepsilon}_{kl}, \tag{3}$$

where $\tilde{\sigma}_{ij} = \sigma_{ij} - \sigma^*_{ij}$, $\tilde{\varepsilon}_{ij} = \frac{1}{2}\left(\tilde{u}_{i,j} + \tilde{u}_{j,i}\right)$ and L_{ijkl} a fourth order tensor depending on the constitutive behavior of the material at the reference state, where the linearization is made. Injecting equation (3) into equation (1) we obtain:

$$L_{ijkl} \tilde{u}_{k,lj} = \rho \ddot{\tilde{u}}_i. \tag{4}$$

The above PDE is linear and can be solved by separation of variables (or Fourier transform). Setting $\tilde{u}_i = X(x_k) U_i(t)$, equation (4) becomes:

$$L_{ijkl} X_{,lj} U_k = \rho X \ddot{U}_i. \tag{5}$$

The general solution of equation (5) in terms of U_i is $U_i = U_i(t) = g_k e^{st}$ leading to:

$$\left(L_{ijkl} X_{,lj} - \rho X s^2 \delta_{ik}\right) g_k = 0, \tag{6}$$

where δ_{ij} is the Kronecker delta.

2.3 Deformation bands

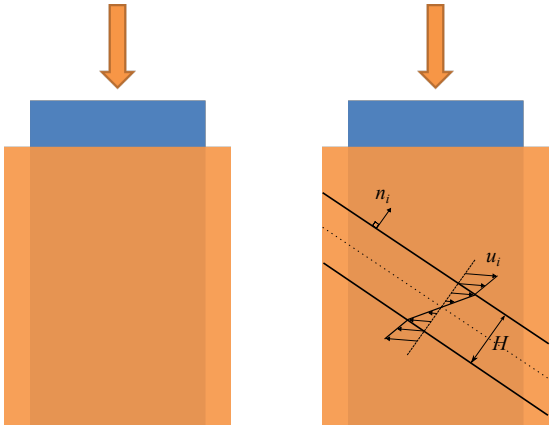

Figure 4: Schematic representation of homogeneous (left) and localized deformation (right) in the form of a band. Blue indicates the initial undeformed state and orange the final form. The loading is applied slowly in a quasistatic manner such as to always satisfy equilibrium $\sigma^*_{ij,j} = 0$. A bifurcation from the equilibrium state with homogeneous deformation to another equilibrium state of non-homogeneous deformation can occur under the conditions of described by equation (8).

Figure 4 shows the formation of a deformation band. As explained below, shear, compaction and dilation bands are all deformation bands. The kinematics for the formation of a deformation band determine the form of the perturbation $\tilde{u}_i$ and consequently X, which has to be a planar wave propagating in direction n_i, i.e. $X(x_k) = e^{\mathrm{i}kn_ix_i}$. $k = \frac{2\pi}{\lambda}$ is the wave number of the perturbation, λ its wavelength and $\mathrm{i} = \sqrt{-1}$. Therefore, the perturbation $\tilde{u}_i$ takes the form:

$$\tilde{u}_i = g_i e^{st+\mathrm{i}kn_jx_j} \tag{7}$$

and equation (6) becomes:

$$\left(\Gamma_{ik} - \rho c^2 \delta_{ik}\right) g_k = 0, \tag{8}$$

where $\Gamma_{ik} = n_j L_{ijkl} n_l$ is the so-called *acoustic tensor*, $c = \mathrm{i}\frac{\lambda s}{2\pi}$ is the propagation velocity of the sinusoidal plane wave described by $\tilde{u}_i = U_i e^{\mathrm{i}kn_ix_i+st}$. The above condition for strain localization coincides with the bifurcation conditions determined in [RR75] (see also Appendix A) and takes the form of a classical eigenvalue problem. The above eigenvalue problem has three eigenvalues $q^{(i)}$ corresponding to three eigenvectors $\{g_k^{(m)}\}$ $(m = 1, 2, 3)$. Given the eigenvalues and solving for the propagation velocity we get $c^{(m)} = \sqrt{\frac{q^{(m)}}{\rho}}$. The Lyapunov exponent is then $s^{(m)} = -\mathrm{i}\frac{2\pi}{\lambda}\sqrt{\frac{q^{(m)}}{\rho}}$. If an $s^{(m)}$ with positive real part exists, i.e. $Re(s^{(m)}) > 0$, then the homogeneous

solution u_i^* is unstable and the system bifurcates to a non-uniform solution, a deformation band, with direction n_i. Strain localization takes place. The type of the defor-

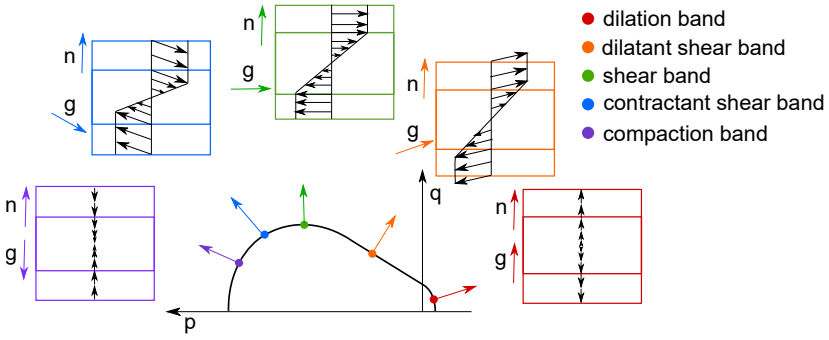

Figure 5: n_i and g_i for different types of deformation bands.

mation band (compaction, shear, dilation band) is determined by the product $n_i g_i$. If $n_i g_i = 0$, the deformation is a shear band, if $n_i g_i = -1$ a pure compaction band and if $n_i g_i = +1$ a pure dilation (extension) band. The intermediate states, $-1 < n_i g_i < 0$ and $0 < n_i g_i < +1$ correspond to contractant and dilatant shear bands, respectively. This is schematically shown in figure 5. More precisely, for an elastoplastic material whose plastic behavior is a function of the first and second invariants of the stress tensor (figure 6), it can be shown that under axisymmetric compression conditions of loading, strain localization occurs when the hardening modulus becomes lower than a critical value h_{cr} for given values of friction coefficient μ and dilatancy β (see figure 7 and [IR00]).

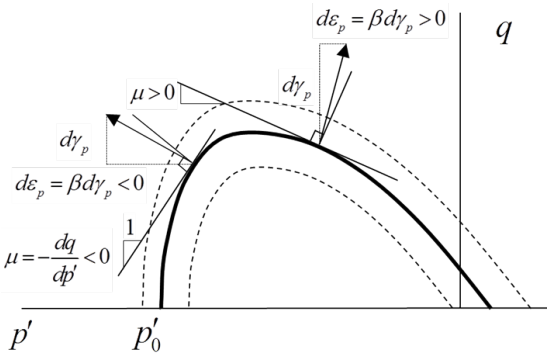

Figure 6: Elastoplastic yield envelope with hardening/softening (dotted lines). Compression is considered negative.

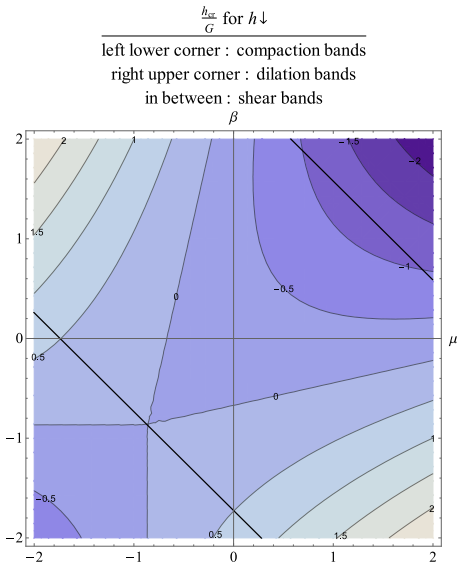

Figure 7: Critical hardening values in function of friction coefficient μ and dilatancy β for strain localization [IR00]. Notice that for non-associate plastic flow rule, localization can occur even with hardening ($h_{cr} > 0$).

2.4 Mesh-size dependency

With the exception of some special cases of constitutive laws that are out of the scope of the present chapter, the acoustic tensor Γ_{ik} does not depend on the (perturbation) wavelength, λ. Therefore, its eigenvalues, $q^{(m)}$ will not depend on λ either. Consequently, the Lyapunov exponent s becomes maximum for decreasing λ ($s^{(m)} = -\mathrm{i}\frac{2\pi}{\lambda}\sqrt{\frac{q^{(m)}}{\rho}}$). In particular $s \to \infty$ for $\lambda \to 0$. This means that the dominant perturbation in time is the one with the smallest wavelength ($\tilde{u}_i = U_i e^{\mathrm{i}kn_i x_i + st}$). In other words the minor imperfection in size in the medium will grow faster and dominate over the other imperfections of larger wavelength. This is why in the classical Cauchy continuum, which has no internal lengths (the acoustic tensor Γ_{ik} does not depend on λ), the deformation band thickness is zero. This means that strain localization takes place on a mathematical plane. The fact that the smallest perturbation propagates faster justifies also mesh-size dependency in Finite Element calculations, if one associates the mesh size with the characteristic wavelength of the perturbation. For instance, in the frame of classical simulations in elastoplasticity of Cauchy rate-independent continua with softening behavior (or even in perfect plasticity), the numerically predicted shear band thickness depends on the finite element discretization and on the element size (figure 8).

It is worth emphasizing that the above condition for strain localization‘is independent

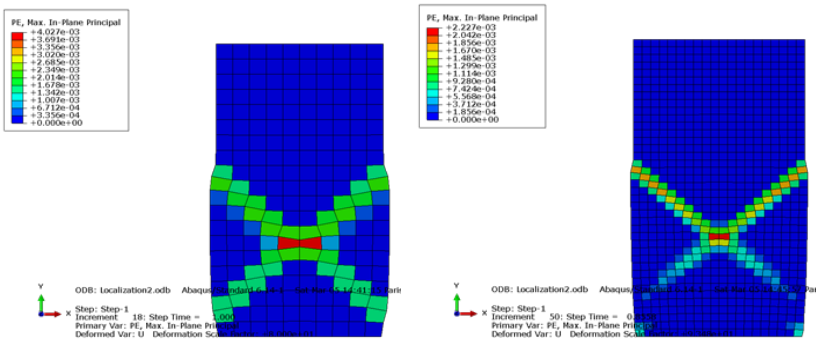

Figure 8: Shear band formation and mesh-size dependency for a rate-independent elastoplastic, von Mises, Cauchy medium with strain softening. The shear band thickness is always 1-2 elements thick and therefore mesh dependent. The plastic strains and the global energy dissipation are also mesh dependent.

of the specific constitutive law, provided that the material is rate-independent and that equation (3) can be written. Rate-dependent materials are treated in the next section where a similar approach is followed for studying strain localization. The above methodology is quite general and can be applied in many problems, including problems with multiphysical couplings, such as thermo-poro-chemo-mechanical couplings (e.g. [Ste14, Sul15]). Moreover, even though a Cauchy (Boltzmann) continuum was considered here, the same approach can be applied in Cosserat or even higher order continua (e.g. [Müh88, Sul11]) as shown in the next Sections.

2.5 1D example

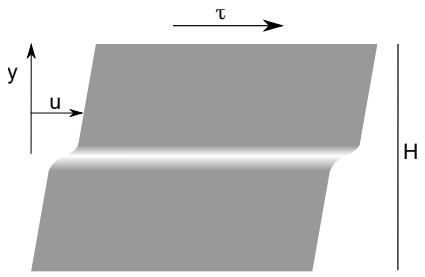

Figure 9: Simple shear of an infinite layer.

In this paragraph we present a simple one dimensional example in order to illustrate the above theoretical notions. We consider a layer that is sheared as shown in figure

9. For the material of the layer we consider an elastoplastic constitutive behavior with mechanical softening. The yield surface is defined as:

$$F = \sigma_{12} - \tau_0 \leq 0, \tag{9}$$

The strain increments are split in elastic and plastic parts as follows (small deformations):

$$\dot{\varepsilon}_{ij} = \dot{\varepsilon}^{el}_{ij} + \dot{\varepsilon}^{pl}_{ij}. \tag{10}$$

In a linear, elastic, isotropic Cauchy medium, the stresses are related to the elastic deformations as follows:

$$\sigma_{ij} = K\varepsilon^{el}_{kk}\delta_{ij} + 2G\left(\varepsilon^{el}_{ij} - \frac{1}{3}\varepsilon^{el}_{kk}\delta_{ij}\right), \tag{11}$$

where K is the bulk modulus and G is the shear modulus. In this 1D example the system is invariant in x_1 and x_3 directions and, therefore, the momentum balance equations become:

$$\frac{\partial \sigma_{12}}{\partial x_2} = \rho\ddot{u}_1; \quad \frac{\partial \sigma_{22}}{\partial x_2} = \rho\ddot{u}_2. \tag{12}$$

We assume that at steady state (equilibrium) we have homogeneous shear. In particular, $\sigma_{12} = \sigma^*_{12} = \tau_0$, $\sigma_{22} = \sigma^*_{22} = \sigma_0$. This state will be stable as long as any perturbation does not grow in time. By perturbing the displacement fields ($u_i = u^*_i + \tilde{u}_i$) Equations (12) become:

$$\frac{\partial \tilde{\sigma}_{12}}{\partial x_2} = \rho\ddot{\tilde{u}}_1; \quad \frac{\partial \tilde{\sigma}_{22}}{\partial x_2} = \rho\ddot{\tilde{u}}_2. \tag{13}$$

For elastoplasticity with mechanical softening (equation (9)):

$$\begin{aligned} \tilde{\sigma}_{12} &= 2G\frac{h}{1+h}\tilde{\varepsilon}_{12} \\ \tilde{\sigma}_{22} &= M\tilde{\varepsilon}_{22}, \end{aligned} \tag{14}$$

where $M = K + \frac{4G}{3}$ is the p-wave elastic modulus and $h = \frac{1}{G}\frac{d\tau_0}{dq} > -1$ is the hardening modulus, with $\dot{q} = \dot{\varepsilon}^{pl}_{(12)}$. $h < 0$ denotes softening.

The perturbations $\tilde{u}_i$ have to fulfill the boundary conditions: $\tilde{\sigma}_{12}\left(x_2 = \pm\frac{H}{2}\right) = \tilde{\sigma}_{22}\left(x_2 = \pm\frac{H}{2}\right) = 0$. H is the height of the sheared layer. Equations (13) and (14) together with the above boundary conditions form a linear system, which admits solutions of the form of Eqs.(7) with $\{n_i\} = \{0, 1, 0\}$. Replacing into equations (13) and solving for s as described in the previous sections, we obtain:

$$s = \mathrm{i}kv_p \quad \text{or} \tag{15}$$

$$s = \pm\mathrm{i}kv_s\sqrt{\frac{h}{h+1}}, \tag{16}$$

where $v_p = \sqrt{\frac{M}{\rho}}$ is the p-wave velocity. The system is unstable when $Re[s] > 0$ or, equivalently when $h < 0$ (softening). As expected, the growth coefficient s becomes infinite for $\lambda \to 0$, which leads to mesh-size dependency.

3 Viscous regularization - characteristic time

Materials whose mechanical response depends on the rate of deformation, as well as on the deformation itself, are referred to as viscous or rate-dependent. The general expression without considering path dependence reads $\sigma_{ij} = \sigma_{ij}\left(\varepsilon_{ij}, \dot{\varepsilon}_{ij}\right)$. The linearized form of the constitutive law around a reference state of homogeneous deformation (see above) reads:

$$\tilde{\sigma}_{ij} = L_{ijkl}\tilde{\varepsilon}_{kl} + M_{ijkl}\dot{\tilde{\varepsilon}}_{kl}. \tag{17}$$

Injecting in the balance equation we obtain:

$$L_{ijkl}\tilde{u}_{k,lj} + M_{ijkl}\dot{\tilde{u}}_{k,lj} = \rho\ddot{\tilde{u}}_i. \tag{18}$$

Using separation of variables (or Fourier transform) we can solve the above linear equation. Limiting our analysis to deformation bands, the perturbation field is given by equation (7). The balance equation now becomes:

$$-n_j L_{ijkl} n_l k^2 g_k XU - n_j M_{ijkl} n_l s k^2 g_k XU - \rho s^2 g_k XU = 0 \tag{19}$$

and finally:

$$\left[n_j L_{ijkl} n_l + n_j M_{ijkl} n_l s + \rho\left(\frac{s}{k}\right)^2 \delta_{ik}\right] g_k = 0 \tag{20}$$

Drawing a parallel to the acoustic tensor, a corresponding second order tensor can be defined for the quantity $n_j M_{ijkl} n_l$. It should however be noted that there is a difference in units. The parallel for the viscous response can then be introduced as $\Delta_{ik} = n_j M_{ijkl} n_l$ leading to:

$$\left(\Gamma_{ik} + \Delta_{ik} s - \rho c^2 \delta_{ik}\right) g_k = 0. \tag{21}$$

3.1 Scaling: Characteristic time and length

To determine the characteristic times, the following quantities are introduced

$$\tau = \frac{t}{T}, \quad \chi_k = \frac{x_k}{L}, \tag{22}$$

where T is a characteristic time for the problem and L a characteristic length (e.g. the height H of the sheared layer of figure 9. Introducing these quantities into equation (21) and dividing by the shear modulus G yields:

$$\left[\frac{\Gamma_{ik}}{G} + \frac{\Delta_{ik}}{GT}\hat{s} + \left(\frac{L}{v_s \hat{k} T}\right)^2 \hat{s}^2 \delta_{ik}\right] g_k = 0, \tag{23}$$

where v_s is the shear-wave velocity, $v_s = \sqrt{\frac{G}{\rho}}$, $\hat{s} = sT$ and $\hat{k} = kL$.

Case 1: Characteristic time due to viscosity

Let us assume that viscosity is dominant. In other words $\frac{\Gamma_{ik}}{G}$ and $\frac{\Delta_{ik}}{GT}$ are terms of $O(1)$ and $\frac{L^2}{v_s^2\hat{k}^2T^2}$ of $O(\varepsilon)$, $\varepsilon \ll 1$. We will determine the characteristic time T_{visc} for this case. $\frac{\Delta_{ik}}{GT_{visc}} = c_{ik} \approx O(1)$ leads to:

$$T_{visc} = c_{ik}\frac{\Delta_{ik}}{G}. \tag{24}$$

Moreover, by hypothesis $\frac{L^2}{v_s^2\hat{k}^2T^2} \ll 1$ and therefore:

$$T_{visc} \gg \frac{L}{v_s\hat{k}} \Rightarrow c_{ik}\frac{\Delta_{ik}}{G} \gg \frac{L\hat{\lambda}}{v_s 2\pi} \Rightarrow$$

$$\hat{\lambda} \ll 2\pi v_s \frac{c_{ik}\Delta_{ik}}{GL} \equiv \hat{\lambda}^*. \tag{25}$$

In other words, when $\lambda \ll \lambda^*$ the inertia terms in equation (23) can be dropped, resulting in:

$$\left(\frac{\Gamma_{ik}}{G} + \frac{\Delta_{ik}}{G}\frac{\hat{s}}{T_{visc}} + \varepsilon\hat{s}^2\delta_{ik}\right) g_k = 0 \Rightarrow \tag{26}$$

$$\left(\frac{\Gamma_{ik}}{G} + c_{ik}s\right) g_k = 0. \tag{27}$$

Assuming strain localization in an isotropic rock with $G \approx 30\text{GPa}$, $c_{ij}\Delta_{ij} = \eta \approx 20\text{MPas}$ and $v_s \approx 2000\text{m/s}$, $\lambda^* \simeq 8m$, which is much bigger than the localization thickness in a deformation band that is of the order of some millimeters or even smaller. Therefore, for typical applications, one would expect viscosity effects to be dominant over inertial ones. This is also shown in the numerical examples in the next paragraph.

Case 2: Characteristic time due to inertia

Suppose that inertia terms are dominant over viscosity. In this case $\frac{\Gamma_{ik}}{G}$ and $\frac{L^2}{v_s^2\hat{k}^2T^2}$ are terms of $O(1)$ and $\frac{\Delta_{ik}}{GT}$ of $O(\varepsilon)$.

From $\frac{L^2}{v_s^2\hat{k}^2T^2} \approx O(1)$ it results that:

$$T_{iner} = \frac{L}{v_s\hat{k}} = \frac{\hat{\lambda}L}{2\pi v_s}. \tag{28}$$

$\frac{\Delta_{ik}}{GT} \ll 1$ yields:

$$c_{ik}\frac{\Delta_{ik}}{G} \ll T_{iner} = \frac{\hat{\lambda}L}{2\pi v_s} \Rightarrow$$

$$\hat{\lambda} \gg \hat{\lambda}^* = 2\pi v_s \frac{c_{ik}\Delta_{ik}}{GL}. \tag{29}$$

Equation (29) means that for very large wave lengths, inertia effects are dominant to viscosity and the second term of equation (23) can be dropped:

$$\left(\frac{\Gamma_{ik}}{G} + s^2\delta_{ik}\right) g_k = 0. \tag{30}$$

Based on the above scalings one -practically- characteristic length, λ^*, was identified and two time scales T_{visc} and T_{iner}. However, there is one more length scale that could be identified.

Case 3: Time scale of negligible rate-independent terms

Of interest is the third and final combination, where both viscosity and inertia are dominant over rate-independent behavior.

We assume a new time-scale, such that $\tau_{v\&i} = \varepsilon^{-a}\tau$. This leads to:

$$\left[\frac{\varepsilon^a\Gamma_{ik}}{G} + \frac{\Delta_{ik}}{GT}\hat{s} + \varepsilon^{-a}\left(\frac{L}{v_s\hat{k}T}\right)^2 \hat{s}^2\delta_{ik}\right] g_k = 0 \tag{31}$$

Assuming $\varepsilon^{-a}\left(\frac{L}{v_s\hat{k}T}\right)^2$ and $\frac{\Delta_{ik}}{GT}$ are terms of $O(1)$ and $\varepsilon^a\frac{\Gamma_{ik}}{G}$ of $O(\varepsilon)$ with $\varepsilon \ll 1$ we obtain that $a = 1$, $T = T_{visc}$ and $\varepsilon = \frac{L^2}{v_s^2\hat{k}^2T^2} = \frac{T_{inertia}^2}{T_{visc}^2}$. Therefore we get:

$$\left(\frac{\varepsilon\Gamma_{ik}}{G} + c_{ik}\hat{s} + \hat{s}^2\delta_{ik}\right) g_k = 0 \Rightarrow \tag{32}$$

$$\left(c_{ik}\hat{s} + \hat{s}^2\delta_{ik}\right) g_k = 0 \tag{33}$$

and

$$T_{v\&i} = \varepsilon T_{visc} = \frac{T_{iner}^2}{T_{visc}} < T_{inner} < T_{visc} \tag{34}$$

Which time scale is more important than the others, depends on the application at hand (e.g. loading conditions, material parameters, localization thickness, imperfections etc.). For a given application, the above scaling laws can considerably simplify the calculations and give physical insight to the results.

3.2 Effects of viscosity and inertia

In one dimension equation (21) reduces to:

$$\Gamma + \Delta s + \frac{\rho}{k^2}s^2 = 0. \tag{35}$$

The question to be answered is for which value of k does s receive its maximum value. The solution to the above equation for $\Gamma = 0$ is $s = 0$ for any value of k and

$$s = -\frac{\Delta k^2}{\rho} \tag{36}$$

is negative for any value of k other than 0, which corresponds to an infinite wavelength.

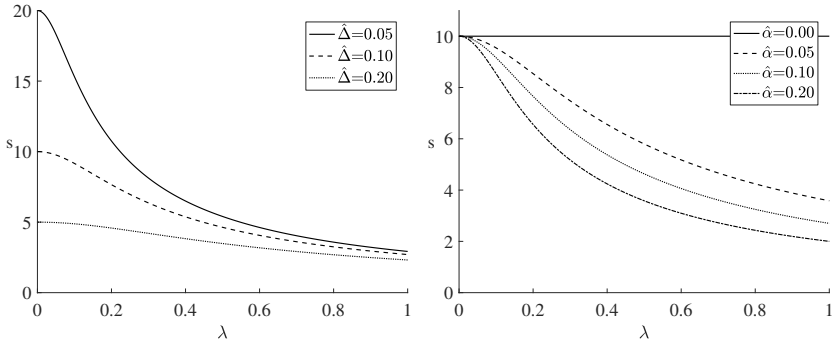

(a) $\hat{\alpha}$=0.1. (b) $\hat{\Delta}$=0.1.

Figure 10: s versus λ for different values of $\hat{\alpha}$ and $\hat{\Delta}$.

If Γ is not equal to zero, there is no loss in generality in dividing by Γ. Substituting in $\lambda = 2\pi/k$ then yields:

$$-1 + \frac{\Delta}{\Gamma}s + \frac{\rho\lambda^2}{4\pi^2\Gamma}s^2 = 0 \Rightarrow \tag{37}$$

$$-1 + \hat{\Delta}s + \hat{\alpha}\lambda^2 s^2 = 0. \tag{38}$$

The solutions to the above quadratic equation are:

$$s_{1,2} = \frac{-\hat{\Delta} \pm \sqrt{\hat{\Delta}^2 + 4\hat{\alpha}\lambda^2}}{2\hat{\alpha}\lambda^2}. \tag{39}$$

Of the two solutions only the one, corresponding to the plus sign, has a positive real part. This is plotted in figure 10 for different values of the quantities $\hat{\Delta}$ and $\hat{\alpha}$. It can be observed that the maximum value of s corresponds in all cases to $\lambda = 0$. In contrast to what was discussed in section 2.4 for the case without any regularization, the maximum value of s is now finite and in fact equal to $1/\hat{\Delta}$. This is illustrated in figure 10a.

It can be further observed that larger values of inertia, represented by the term $\hat{\alpha}$, correspond to a more rapid decrease in the value of s with increasing values of α. This is particularly easy to note in figure 10b.

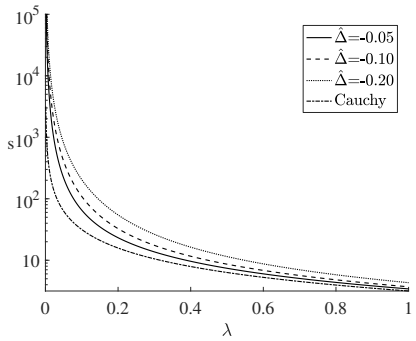

Figure 11: s versus λ for different negative values of $\hat{\Delta}$ and for $\hat{\alpha}$=0.1.

Up to this point it has been tacitly assumed that the contribution of the viscosity has been positive, in the sense that the material exhibits strain rate hardening, rather than strain rate softening. This is the case when the eigenvalues of Δ_{ij} in two- or three-dimensions or the value of $\hat{\Delta}$ in one dimension are positive. It is however also possible that a material may exhibit strain rate softening. For the one dimensional case its effect is illustrated in figure 11. As may be observed, the maximum value of the growth coefficient s goes to infinity as $\lambda \to 0$ and in fact does so faster than in the case of the Cauchy continuum.

3.3 1D Example

The example considered in section 2.5 is revisited here, incorporating a viscous material response. The sheared layer of figure 9 is considered. The material response is assumed to be elasto-viscoplastic with the yield function given in equation (9) and the elastic response given in equation (11). The strain increments are split in elastic and viscoplastic parts as follows (small deformations):

$$\dot{\varepsilon}_{ij} = \dot{\varepsilon}^{el}_{ij} + \dot{\varepsilon}^{vpl}_{ij}. \tag{40}$$

with the viscoplastic strain increments described by a Perzyna type model [Per66]:

$$\dot{\varepsilon}^{vp}_{ij} = \dot{\lambda}\frac{\partial F}{\partial \sigma_{ij}} = \frac{F}{\eta f_0}\frac{\partial F}{\partial \sigma_{ij}}, \tag{41}$$

where η is a constant with units of time, indirectly expressing viscosity, and f_0 is a constant with units of stress, commonly the initial value of the material parameter τ_0. The balance equations are the same as in equations (12) and (13) for the unperturbed and the perturbed states respectively.

From the definition of the plastic multiplier $\dot{\lambda}$ in equation (40) it results that:

$$\dot{F} = \eta f_0 \ddot{\lambda} \Rightarrow \tag{42}$$

$$\dot{\sigma}_{12} = 2G\frac{h}{1+h}\dot{\varepsilon}_{12} + \frac{\eta f_0}{1+h}\ddot{\lambda}. \tag{43}$$

From the definition of the viscoplastic strain and the form of the yield function it results that $\ddot{\lambda} = \ddot{\varepsilon}_{12}^{vp}$. Moreover, the first time derivative can be substituted with a perturbation by considering time integration and successive perturbation. The result reads:

$$\tilde{\sigma}_{12} = 2G\frac{h}{1+h}\tilde{\varepsilon}_{12} + 2\frac{\eta f_0}{1+h}\dot{\tilde{\varepsilon}}_{12}^{vp} \Rightarrow \tag{44}$$

$$\tilde{\sigma}_{12} = 2G\frac{h}{1+h}\tilde{\varepsilon}_{12} + 2\frac{\eta f_0}{1+h}\dot{\tilde{\varepsilon}}_{12} - \frac{\eta f_0}{G(1+h)}\dot{\tilde{\sigma}}_{12}. \tag{45}$$

Making use of equation (43) in equation (45) in the form of successive substitutions yields

$$\tilde{\sigma}_{12} = 2G\frac{h}{1+h}\tilde{\varepsilon}_{12} + 2\frac{\eta f_0}{(1+h)^2}\dot{\tilde{\varepsilon}}_{12} - 2\frac{(\eta f_0)^2}{G(1+h)^3}\ddot{\tilde{\varepsilon}}_{12} + 2\frac{(\eta f_0)^3}{G^2(1+h)^4}\dddot{\tilde{\varepsilon}}_{12} - \dots \tag{46}$$

It can be observed that the above is an infinite series with alternating sign of coefficients. The coefficients follow a geometric progress where the multiplier is equal to $\frac{\eta f_0}{G(1+h)}$. To maintain an analogy to equation (17) only the first two terms on the right hand side of the equation are retained. On the whole the constitutive law now reads:

$$\begin{aligned} \tilde{\sigma}_{12} &= 2G\frac{h}{1+h}\tilde{\varepsilon}_{12} + 2\frac{\eta f_0}{(1+h)^2}\dot{\tilde{\varepsilon}}_{12} \\ \tilde{\sigma}_{22} &= M\tilde{\varepsilon}_{22}, \end{aligned} \tag{47}$$

where, again, $M = K + \frac{4G}{3}$ is the p-wave elastic modulus and $h = \frac{1}{G}\frac{d\tau_0}{dq} > -1$ is the hardening modulus.

Following the analysis presented in section 2.5 from the first balance equation we obtain:

$$G\frac{h}{1+h}k^2 + \frac{\eta f_0}{(1+h)^2}k^2 s + \rho s^2 = 0 \Rightarrow \tag{48}$$

$$v_s^2\frac{h}{1+h}k^2 + v_s^2\frac{\eta f_0}{G(1+h)^2}k^2 s + s^2 = 0 \tag{49}$$

Solving for s yields:

$$s = -\frac{1}{2}v_s^2\frac{\eta f_0}{G(1+h)^2}k^2 \pm \frac{1}{2}\sqrt{\left(v_s^2\frac{\eta f_0}{G(1+h)^2}k^2\right)^2 - 4v_s^2\frac{h}{1+h}k^2}. \tag{50}$$

On the whole, from both balance equations we obtain:

$$s = \mathrm{i}kv_p \quad \text{or} \tag{51}$$

$$s = -v_s^2\frac{\eta f_0}{2G(1+h)^2}k^2 \pm \sqrt{\left(v_s^2\frac{\eta f_0}{2G(1+h)^2}k^2\right)^2 - v_s^2\frac{h}{1+h}k^2}, \tag{52}$$

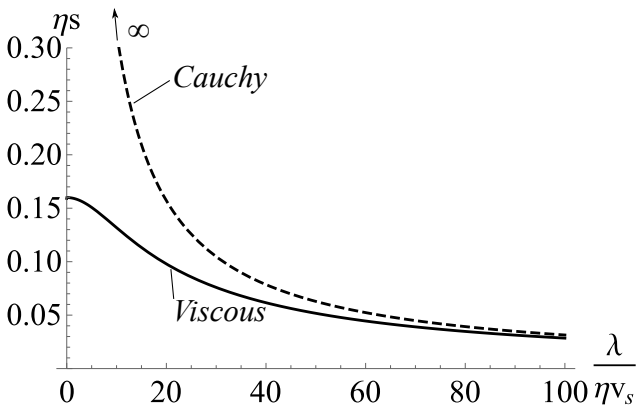

Figure 12: Growth coefficient in function of the perturbation wavelength. Contrary to Cauchy continuum, the maximum value of the growth coefficient is finite.

where $v_p = \sqrt{\frac{M}{\rho}}$ is the p-wave velocity and $v_s = \sqrt{\frac{G}{\rho}}$ is the s-wave velocity. The system is unstable when $Re[s] > 0$ and it reduces to the solution given in section 2.5 when $\eta = 0$.

A comparison to the Cauchy continuum is presented in figure 12. For $\eta \neq 0$, we observe that the growth coefficient s becomes maximum for $\lambda = 0$, but non infinite as in the case of rate-independent materials. In other words the presence of a characteristic time due to viscosity limits the growth coefficient and consequently perturbations propagate in finite time. Moreover, in the absence of inertia (or if it is very small, see scaling, paragraph 3.1) the growth coefficient is finite and independent of the wave length of the perturbation (see figure 10 for $\hat{\alpha}$). The consequence of this latter observation is that in numerical analyses the results are mesh-independent [Nee88, WSD96]. However, they depend on existing perturbations related to the material parameters (e.g. imperfections) or the loading conditions which might favor one wave-length or another.

4 Micromorphic continua regularization - characteristic lengths

The theory of Micromorphic continua is a general continuum theory that can represent various heterogeneous systems with microstructure of non-negligible size and take into account various length and time scales (internal lengths) that the classical Cauchy continuum fails to represent. The various features of the Micromorphic continuum theory were studied by many researchers in the past, showing several advan-

tages compared to the classical continuum approach. Intrinsic wave dispersion, non-singular fields in fracture mechanics, interesting properties related to the design of metamaterials, are some of the applications that emerge from the deep study of these continua. Regularization in strain localization problems is another feature of these continua due to the characteristic lengths they embody.

According to Germain [Ger73b] the Cauchy continuum is a continuous distribution of particles, each of them being represented geometrically by a point and characterized kinematically by a velocity V_i. In a theory that takes microstructure into account each particle has kinematic properties that are defined in a more detailed way.

At the microscopic level of observation, a particle appears itself as a continuum $P(M)$ of small extent. Let M be the center of mass of the particle $P(M)$, M' a point of $P(M)$, u_i the displacement of M (V_i its velocity), x'_i the coordinates of M' in a Cartesian frame parallel to the given, global frame and M its origin, u'_i the displacement of M' with respect to the given frame (V'_i its displacement) and x_i the coordinates of M in the given frame (see figure 13). D denotes the control volume. As $P(M)$ is of small extent, it is natural to look at the asymptotic expansion of V'_i with respect to x'_i:

$$u'_i = u_i + \chi_{ij}x'_j + \chi_{ijk}x'_jx'_k + \chi_{ijkl}x'_jx'_kx'_l + \dots, \tag{53}$$

where χ_{ij} is a micro-deformation tensor, which expresses the gradient of the relative displacements u'_i and $\chi_{ij\dots m}$ are higher order micro-deformation rate tensors. In three-dimensions: $i, j, \dots, m = 1, 2, 3$. The tensors $\chi_{ij\dots m}$ are assumed to be fully symmetric with respect to the indices $j, \dots, m$.

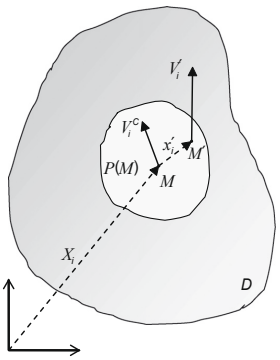

Figure 13: Continuum with microstructure.

Applying the principle of virtual power and using the divergence theorem (see [Ger73b]

and [Ste18] for more details on derivation), we obtain:

$$\begin{aligned} \tau_{ij,j} + f_i &= 0, & t_i &= \tau_{ij} n_j \\ \nu_{ijk,k} + s_{ij} + \psi_{ij} &= 0, & \mu_{ij} &= \nu_{ijk} n_k \\ \nu_{ijkl,l} + s_{ijk} + \psi_{ijk} &= 0, & \mu_{ijk} &= \nu_{ijkl} n_l \\ &\dots, \end{aligned} \tag{54}$$

where, again, n_i is the outward pointing unit normal vector field of the boundary of the solid. The above system of equations represents the equilibrium equations of a Micromorphic continuum of order n (strong form).

The additional degrees of freedom of Micromorphic continua introduce microinertia terms, whose presence leads to interesting wave dispersion properties, especially at short wavelengths (optic branch) [SSV10] and finite Lyapunov exponents in localization problems [SSV11].

In figure 14 we outline the various higher order (Micromorphic) continuum theories and their special cases. Besides the classical continuum and the Cosserat continuum (called also micropolar continuum, see [Var09]), a special case of Micromorphic continuum is also the second gradient and the indeterminate couple stress theory (called also restrained Cosserat medium).

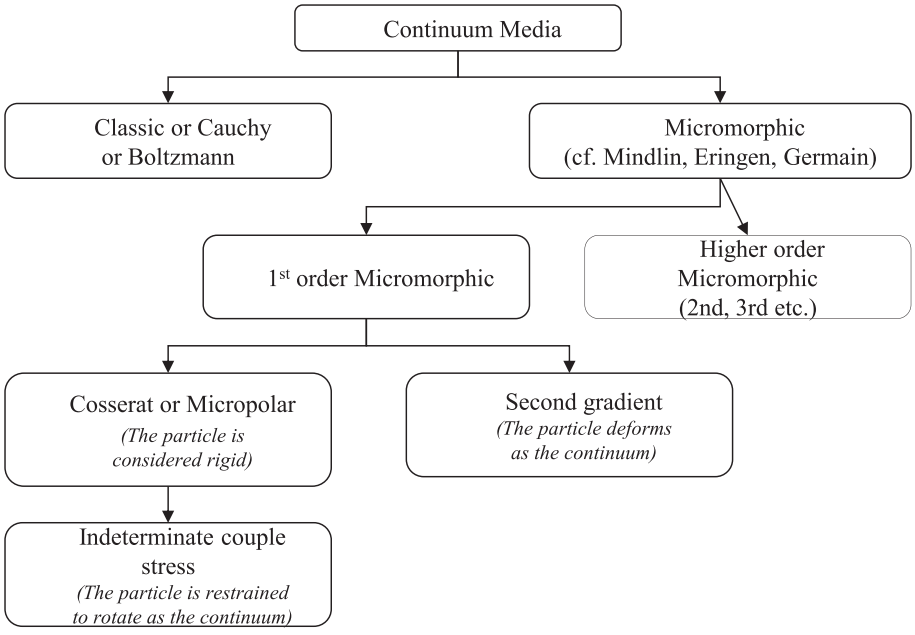

Figure 14: Higher order continuum theories according to Germain's terminology [Ger73b]; see also [Min64, Eri99].

Retrieving the classical, Boltzmann continua, is straightforward by setting χ_{ij} and the higher order microdeformation rate tensors null. In this case, $s_{ij} = 0$ and $\tau_{ij} = \sigma_{ij}$, i.e. equal to the Cauchy stress tensor, which is symmetric.

In the case that the particle $P(M)$ is deformable and its microdeformation coincides with the deformation of the (macro-)continuum, i.e. $\chi_{ij} = V_{i,j}$, we obtain the so-called second gradient continuum theory. As in this case the microdeformation rate tensor is no more an independent generalized virtual velocity, one has to start from the very beginning and apply the principle of virtual power for deriving the strong form of the equilibrium equations and the appropriate boundary conditions. For more details we refer to [Ger73b] and for some interesting applications of the theory to [DSMP93, CCE98, ZPV01, CCC06, SDC07, KABC08, PZ16, DAD+17], among others. Alternatively, second gradient continua can be derived by assuming that the internal energy depends explicitly on the second gradient of the displacement field [Ger73a, Min65]. As fat it concerns strain localization, second gradient continuum leads to deformation bands of finite thickness and remedies mesh dependency in finite element analyses. For a more detailed study of second gradient theories related to strain localization we refer to [CCM01, CCC06].

4.1 Cosserat continuum

The derivation of the Cosserat continuum is more direct than the second gradient. The basic assumption is that the particle $P(M)$ behaves as a rigid body and so it can not only translate, but also rotate. In this case the microdeformation rate tensor has to be anti-symmetric and the rest higher-order microdeformation tensors zero.

Adding inertia effects and neglecting volumic forces, equilibrium equations (equations (54)) become:

$$\begin{aligned} \tau_{ij,j} + f_i &= \rho \ddot{u}_i, \qquad & t_i &= \tau_{ij} n_j \\ m_{ij,j} - \epsilon_{ijk}\tau_{jk} + \psi_i &= I\ddot{\omega}_i^c, \qquad & \mu_i &= m_{ij} n_j. \end{aligned} \tag{55}$$

This is the strong form of the Cosserat continuum equations. τ_{ij} is the Cosserat stress tensor, which is not symmetric and m_{ij} is the Cosserat moment (couple stress) tensor. ϵ_{ijk} is the Levi-Civita symbol. f_i and ψ_i are respectively volumic (body) forces and moments and u_i and ω_i^c are respectively the Cosserat displacements and rotations. t_i and μ_i denote boundary tractions and I is the microinertia.

A constitutive law connects the generalized stresses τ_{ij} and m_{ij} with the generalized deformations γ_{ij} and κ_{ij}:

$$\begin{aligned} \gamma_{ij} &= u_{i,j} + \epsilon_{ijk}\omega_k^c \\ \kappa_{ij} &= \omega_{i,j}^c, \end{aligned} \tag{56}$$

i.e. $\tau_{ij} = \tau_{ij}(\gamma_{ij}, \kappa_{ij})$ and $m_{ij} = m_{ij}(\gamma_{ij}, \kappa_{ij})$. We assume an equilibrium state of homogeneous deformation and search for the conditions where this state becomes

unstable leading to the formation of a deformation band. To this extend, we perturb the kinematic fields u_i and ω_i as follows:

$$\begin{aligned}\tilde{u}_i =& u_i - u_i^* = U_i e^{st+\mathrm{i}kn_j x_j}\\ \tilde{\omega}_i^c =& \omega_i^c - \omega_i^{c*} = \Omega_i e^{st+\mathrm{i}kn_j x_j}.\end{aligned} \tag{57}$$

Linearization of the constitutive law yields (see [RSS18] for an application in elasto-plasticity):

$$\begin{aligned}\tilde{\tau}_{ij} =& C_{ijkl}^{TT}\tilde{\gamma}_{kl} + C_{ijkl}^{TM}\tilde{\kappa}_{kl}\\ \tilde{m}_{ij} =& C_{ijkl}^{MT}\tilde{\gamma}_{kl} + C_{ijkl}^{MM}\tilde{\kappa}_{kl}.\end{aligned} \tag{58}$$

Notice that κ_{ij} has units of deformation over length. Consequently, any ratio of the various tensors C^{XX} produces a characteristic length for the problem at hand. Inserting equations (57) and equations (58) into equations (55) we obtain the following system of algebraic equations:

$$\begin{bmatrix}\Gamma_{ik} + \rho\left(\frac{s}{k}\right)^2\delta_{ik} & \Delta_{ik}\\ \Xi_{ik} & \Pi_{ik} + I\left(\frac{s}{k}\right)^2\delta_{ik}\end{bmatrix}\begin{bmatrix}U_k\\ \Omega_k\end{bmatrix} = 0, \tag{59}$$

where

$$\Gamma_{ik} = n_j C_{ijkl}^{TT} n_l \tag{60}$$

$$\Delta_{ik} = -\mathrm{i}\frac{1}{k} n_j e_{qlk} C_{ijql}^{TT} + n_j C_{ijkl}^{TM} n_l \tag{61}$$

$$\Xi_{ik} = n_j C_{ijkl}^{MT} n_l + \mathrm{i}\frac{1}{k} e_{ijr} C_{jrkq}^{TT} n_q \tag{62}$$

$$\Pi_{ik} = n_j C_{ijkl}^{MM} n_l - \mathrm{i}\frac{1}{k} e_{rnk} C_{ilrn}^{MT} n_l + \frac{1}{k^2} e_{ilr} C_{lrnq}^{TT} e_{nqk} + \mathrm{i}\frac{1}{k} e_{ilr} C_{lrkq}^{TM} n_q. \tag{63}$$

The strain localization condition for deformation bands in the framework of Cosserat continuum is:

$$\mathrm{Det}\left(\begin{bmatrix}\Gamma_{ik} - \rho c^2\delta_{ik} & \Delta_{ik}\\ \Xi_{ik} & \Pi_{ik} - Ic^2\delta_{ik}\end{bmatrix}\right) = 0. \tag{64}$$

The singularity of the above tensor is similar to the condition found in [IW98, SW91] for the onset of localization ($s = 0$). In these papers, the authors derive the localization condition from the kinematic and static compatibility conditions across the shear band as done classically for strain localization analysis [MV87, VS95]. Note that if no Cosserat effects are considered the classical condition of localization for rate-independent materials with a Cauchy continuum is retrieved, i.e. $\mathrm{Det}(n_j C_{ijkl}^{TT} n_l) = 0$. For more details we refer to [RSS18].

4.2 1D example of regularization with Cosserat continuum

An elastoplastic constitutive behavior with mechanical softening is considered in this example. More advanced Cosserat constitutive models such as the Mühlhaus-Vardoulakis

Cosserat plasticity model [MV87, VS95, RSS18] might be used, but the advantage of this simple and unrealistic for granular material models is that analytical derivations can be performed easily. The yield surface is defined as:

$$F = \tau_{(12)} - \tau_0 \leq 0, \tag{65}$$

where $\tau_{(ij)}$ denotes the symmetric part of the stress tensor τ_{ij}. The strains and curvatures of the Cosserat medium are split in elastic and plastic parts as follows:

$$\begin{aligned} \dot{\gamma}_{ij} &= \dot{\gamma}^{el}_{ij} + \dot{\gamma}^{pl}_{ij} \\ \dot{\kappa}_{ij} &= \dot{\kappa}^{el}_{ij} + \dot{\kappa}^{pl}_{ij}. \end{aligned} \tag{66}$$

In a centrosymmetric, linear elastic isotropic Cosserat medium, the stresses are related to the generalized elastic deformation measures according to the following constitutive relations [Var09]:

$$\begin{aligned} \tau_{ij} &= K\gamma^{el}_{kk}\delta_{ij} + 2G\left(\gamma^{el}_{(ij)} - \frac{1}{3}\gamma^{el}_{kk}\delta_{ij}\right) + 2\eta_1 G\gamma^{el}_{[ij]} \\ m_{ij} &= 4GR^2\left(\kappa^{el}_{(ij)} + \eta_2\kappa^{el}_{kk}\delta_{ij}\right) + 4\eta_3 GR^2\kappa^{el}_{[ij]}, \end{aligned} \tag{67}$$

where η_1, η_2, η_3 are positive material constants and R is an internal length parameter, which for a granular material can be identified with the mean radius of the grains of the Representative Volume Element (RVE). For more details on homogenization approaches tailored to Cosserat continuum and upscaling, both in elasticity and plasticity, the reader is referred to [BV01, GSSS16, RC16]. $\gamma_{(ij)}$ and $\gamma_{[ij]}$ denote respectively the symmetric and anti-symmetric parts of γ_{ij}. The Cosserat shear modulus, which expresses the stiffness related to the relative rotation of the particle (e.g. of a grain) with respect to the macro-rotation of the continuum (e.g. of the assemblage of grains) is defined as $G_c = \eta_1 G$. In this 1D example the system is invariant in x_1 and x_3 directions and, therefore, the momentum balance equations become:

$$\begin{aligned} &\frac{\partial \tau_{12}}{\partial x_2} = \rho\ddot{u}_1; \quad \frac{\partial \tau_{22}}{\partial x_2} = \rho\ddot{u}_2 \\ &\frac{\partial m_{32}}{\partial x_2} + \tau_{21} - \tau_{12} = I\ddot{\omega}^c_3. \end{aligned} \tag{68}$$

At steady state we have a Cauchy continuum under homogeneous shear. In particular, $\tau_{(12)} = \tau^*_{(12)} = \tau_0$, $\tau_{22} = \tau^*_{22} = \sigma_0$, $\tau_{[12]} = \tau^*_{[12]} = 0$ and $m_{32} = m^*_{32} = 0$. This state will be stable as long as any perturbation does not grow in time. By perturbing the displacement and the rotation fields at steady state ($u_i = u^*_i + \tilde{u}_i$, $\omega_3 = \omega^{c*}_3 + \tilde{\omega}^c_3$) equations (68) yield:

$$\begin{aligned} &\frac{\partial \tilde{\tau}_{12}}{\partial x_2} = \rho\ddot{\tilde{u}}_1; \quad \frac{\partial \tilde{\tau}_{22}}{\partial x_2} = \rho\ddot{\tilde{u}}_2 \\ &\frac{\partial \tilde{m}_{32}}{\partial x_2} + \tilde{\tau}_{21} - \tilde{\tau}_{12} = I\ddot{\tilde{\omega}}^c_3. \end{aligned} \tag{69}$$

For elastoplasticity with mechanical softening (equation (65)):

$$\begin{aligned}\tilde{\tau}_{(12)} &= 2G\frac{h}{1+h}\tilde{\gamma}_{(12)}\\ \tilde{\tau}_{[12]} &= 2G_c\tilde{\gamma}_{[12]}\\ \tilde{\tau}_{22} &= M\tilde{\gamma}_{22}\\ \tilde{m}_{32} &= 4GR^2\tilde{\kappa}_{32}.\end{aligned} \tag{70}$$

The perturbations $\tilde{u}_i$ and $\tilde{\omega}_3^c$ have to fulfill the boundary conditions: $\tilde{\sigma}_{12}\left(x_2=\pm\frac{H}{2}\right)=\tilde{\sigma}_{22}\left(x_2=\pm\frac{H}{2}\right)=\tilde{m}_{32}\left(x_2=\pm\frac{H}{2}\right)=0$. H is the height of the sheared layer. Equations (69) and (70) together with the above boundary conditions form a linear system which admits solutions of the form of equations (57) with $\{n_i\}=\{0,1,0\}$. Replacing into equations (69) and solving for s as described in the previous sections, we obtain:

$$s = \mathrm{i}kv_p \quad \text{or} \tag{71}$$

$$s = \pm\mathrm{i}kv_s\sqrt{\frac{h}{h+1}}\sqrt{\frac{\eta_1\left(1+\frac{1}{k^2R^2}\right)+\frac{h+1}{h}}{\frac{\eta_1}{k^2R^2}+1}}, \tag{72}$$

where I was taken equal to zero for simplicity. The system is unstable when $Re[s]>0$ or, equivalently when $h<0$ (softening) and $\eta_1\left(1+\frac{1}{k^2R^2}\right)+\frac{h+1}{h}>0$. The latter condition leads to a critical wavelength λ_{cr}:

$$\lambda > \lambda_{cr} = 2\pi R\sqrt{-\frac{1+h}{h}-\frac{1}{\eta_1}}. \tag{73}$$

The wavelength of the perturbation has to be larger than this critical value for localization to occur. Notice that λ_{cr} is proportional to the Cosserat internal length, R. If $R\to 0$ we retrieve the same condition for strain localization with the 1D example presented in paragraph 2.5 for a Cauchy continnum (see figure 15).

5 Regularization and multiphysics couplings - characteristic length/time

It is often the case that the mechanical response of a given material depends on other physical or chemical processes taking place. Such processes can in turn be influenced by the mechanical response of the material to the changing conditions and to the load, leading for example to changes in porosity or internal structure and producing heat through internal friction. If that is the case one speaks of multi-physical couplings. The processes most commonly taken into account are hydraulic, thermal or chemical.

Materials whose mechanical response depends on a number of additional physical quantities θ_i, $i=1,\ldots,N$, as well as on the deformation, obey the following general

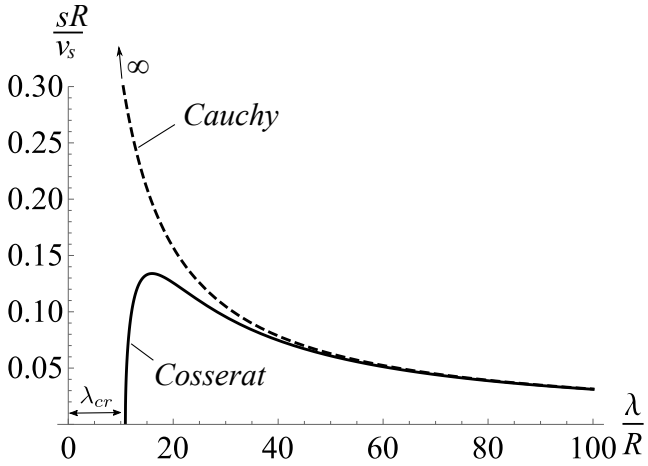

Figure 15: Growth coefficient in function of the perturbation wavelength. Contrary to Cauchy continuum, strain localization is not possible for $\lambda < \lambda_{cr}$ in the case of Cosserat continuum.

expression, when the path dependence is not considered: $\sigma_{ij} = \sigma_{ij}\left(\epsilon_{ij}, \theta_m\right)$. The linearized form of the constitutive law around the a reference state of homogeneous deformation reads:

$$\tilde{\sigma}_{ij} = L_{ijkl}\tilde{\varepsilon}_{kl} + A_{mij}\tilde{\theta}_m. \tag{74}$$

Injecting in the balance equation we obtain:

$$L_{ijkl}\tilde{u}_{k,lj} + A^m_{ij}\tilde{\theta}_{m,j} = \rho\ddot{\tilde{u}}_i. \tag{75}$$

Each of the quantities θ_i obey in turn their own balance equations, which, with little loss in generality we can assume to be of the advection-diffusion type:

$$\left(D^{(i)}\left(u_{m,n}, \theta_k\right)\theta_{i,j}\right)_{,j} - \left(v_j\theta_i\right), j + R^{(i)}\left(u_{m,n}, \theta_k\right) = \dot{\theta}_i, \tag{76}$$

where $D^{(i)}$ is the diffusion coefficient of the quantity θ_i, $R^{(i)}$ is the source or sink term of the same quantity and v_j is the velocity field controlling the advection. When the diffusion coefficient is constant and the advective flow is incompressible, the advection-diffusion equation simplifies to:

$$D^{(i)}\theta_{i,jj} - v_j\theta_{i,j} + R^{(i)}\left(u_{m,n}, \theta_k\right) = \dot{\theta}_i. \tag{77}$$

Expansion of the balance equation (76) leads to the following formulation:

$$\begin{aligned} D^{(i)}\theta_{i,jj} + \frac{\partial D^{(i)}}{\partial u_{m,n}}\theta_{i,j}u_{m,nj} + \frac{\partial D^{(i)}}{\partial \theta_k}\theta_{i,j}\theta_{k,j} \quad &+ \\ -v_{jj}\theta_i - v_j\theta_{i,j} + R^{(i)}\left(u_{m,n}, \theta_k\right) \quad &= \quad \dot{\theta}_i, \end{aligned} \tag{78}$$

where the dependencies of the function $D^{(i)}\left(u_{m,n},\theta_k\right)$ have been omitted for the sake of brevity. Linearization in turn yields:

$$\begin{aligned} & D^{(i)}\tilde{\theta}_{i,jj} \quad + \\ +\frac{\partial D^{(i)}}{\partial u_{m,n}}\theta_{i,j}\tilde{u}_{m,nj} + \frac{\partial D^{(i)}}{\partial u_{m,n}}u_{m,nj}\tilde{\theta}_{i,j} \quad & + \\ +\frac{\partial D^{(i)}}{\partial \theta_k}\theta_{i,j}\tilde{\theta}_{k,j} + \frac{\partial D^{(i)}}{\partial \theta_k}\theta_{k,j}\tilde{\theta}_{i,j} \quad & + \\ -v_{jj}\tilde{\theta}_i - v_j\tilde{\theta}_{i,j} \quad & + \\ +\frac{\partial R^{(i)}}{\partial u_{m,n}}\tilde{u}_{m,n} + \frac{\partial R^{(i)}}{\partial \theta_k}\tilde{\theta}_k \quad & = \quad \dot{\tilde{\theta}}_i, \end{aligned} \tag{79}$$

where the dependencies of the function $R^{(i)}\left(u_{m,n},\theta_k\right)$ have also been omitted. Collecting the terms with the same perturbation components results in:

$$\begin{aligned} D^{(i)}\tilde{\theta}_{i,jj} + P_j^{(i)}\tilde{\theta}_{i,j} - v_{jj}\tilde{\theta}_i + Q_{kj}^{(i)}\tilde{\theta}_{k,j} + \frac{\partial R^{(i)}}{\partial \theta_k}\tilde{\theta}_k \quad & + \\ +S_{mnj}^{(i)}\tilde{u}_{m,nj} + \frac{\partial R^{(i)}}{\partial u_{m,n}}\tilde{u}_{m,n} \quad & = \quad \dot{\tilde{\theta}}_i. \end{aligned} \tag{80}$$

The stability of the system of equations consisting of the above system of equations and equation (75) obviously depends on the values of the prefactors, which however are not known at this point.

The corresponding linearized form for the balance equation (77) reads:

$$D^{(i)}\tilde{\theta}_{i,jj} - v_j\tilde{\theta}_{i,j} + \frac{\partial R^{(i)}}{\partial u_{m,n}}\tilde{u}_{m,n} + \frac{\partial R^{(i)}}{\partial \theta_k}\tilde{\theta}_k = \dot{\tilde{\theta}}_i. \tag{81}$$

The perturbation $\tilde{u}_i$ is assumed to be of the form given in equation (7), while $\tilde{\theta}_i$ is assumed to be given by:

$$\tilde{\theta}_i = h_i e^{st+\mathrm{i}kn_jx_j}. \tag{82}$$

Equations (75), (80) and (81) become:

$$-\left(k^2 n_j L_{ijkl} n_l + s^2\rho\delta_{ik}\right) g_k + \mathrm{i}kA_{kij}n_j h_k = 0 \tag{83}$$

$$\begin{aligned} \left[-k^2 D^{(i)} n_i\delta_{ik} + \mathrm{i}k\left(P_j^{(i)}n_j\delta_{ik} + Q_{kj}^{(i)}n_j\right) + \frac{\partial R^{(i)}}{\partial \theta_k} - \left(v_{jj}+s\right)\delta_{ik}\right] h_k + & \\ + \left(-k^2 S_{kjl}^{(i)} n_j n_l + \mathrm{i}k\frac{\partial R^{(i)}}{\partial u_{k,j}}n_j\right) g_k = 0 & \end{aligned} \tag{84}$$

and

$$\left[\left(-k^2 D^{(i)} - \mathrm{i}kv_j n_j - s\right)\delta_{ik} + \frac{\partial R^{(i)}}{\partial \theta_k}\right] h_k + \mathrm{i}k\frac{\partial R^{(i)}}{\partial u_{k,j}}n_j g_k = 0. \tag{85}$$

respectively. Irrespectively of whether the simplified or the full form of the advection-diffusion equation is used for the multiphysical processes, the system of equations now takes the form:

$$\begin{bmatrix} C_{ik}^{gg} & C_{il}^{gh} \\ C_{ik}^{hg} & C_{il}^{hh} \end{bmatrix} \begin{bmatrix} g_k \\ h_l \end{bmatrix} = \begin{bmatrix} 0 \\ 0 \end{bmatrix}, \tag{86}$$

with

$$C_{ik}^{gg} = -\left(k^2 \Gamma_{ik} + s^2 \rho \delta_{ik}\right) \tag{87}$$

$$C_{ik}^{gh} = \mathrm{i}k A_{kij} n_j \tag{88}$$

$$C_{ik}^{hg} = -k^2 S_{kjl}^{(i)} n_j n_l + \mathrm{i}k \frac{\partial R^{(i)}}{\partial u_{k,j}} n_j \tag{89}$$

$$C_{ik}^{hh} = -k^2 D^{(i)} n_i \delta_{ik} + \mathrm{i}k \left(P_j^{(i)} n_j \delta_{ik} + Q_{kj}^{(i)} n_j\right) + \frac{\partial R^{(i)}}{\partial \theta_k} - \left(v_{jj} + s\right) \delta_{ik}, \tag{90}$$

where the last two equations correspond to the full form of the advection-diffusion equation.

Requiring the determinant of the system of equations to be equal to zero results in a cubic equation in terms of s. The three roots clearly depend on the value of the various multipliers, but some general remarks may be made without introducing numerical values.

No coupling

When the coupling terms C_{ik}^{gh} and C_{ik}^{hg} are ignored, the possible roots are the two roots resulting from the LSA of the stress balance without any regularization and an additional one from the advection-diffusion equation. When considering the advection-diffusion equation with simplifications, it is clear that the real part of this root will be negative as long as the diffusivity coefficient is positive. This is usually the case with some exceptions, such as the consolidation equation when considering a collapsible solid matrix.

One way coupling

Assuming only the physical process to have an effect on the stress balance equation and itself not to be affected, one speaks of one way coupling. Then it is enough to consider the solution of:

$$-k^2 \Gamma - s^2 \rho + \mathrm{i}k A = 0 \tag{91}$$

with respect to s. The solution reads:

$$s = \pm \frac{\sqrt{-k^2 \Gamma + \mathrm{i}k A}}{\sqrt{\rho}} = \pm \frac{\sqrt{-4\pi^2 \Gamma + \mathrm{i}2\pi A \lambda}}{\sqrt{\rho \lambda^2}} = \pm \frac{\sqrt{-\hat{\Gamma} + \mathrm{i}\hat{A}\lambda}}{\lambda}, \tag{92}$$

where solutions with positive real part are principally of interest. It is clear from the above equation that for $\lambda \to 0$ the real part of s goes to infinity, as for the case without regularization.

Two way coupling

When the coupling terms are taken into account a cubic equation results with the coupling terms contributing to the constant term with respect to s. To illustrate the effect of the coupling, the problem is considered in one dimension for a single coupled process for the simplified form of the advection-diffusion equation. For the sake of simplicity the advective term and the influence of θ on the source term are ignored:

$$-\left(k^2\Gamma + s^2\rho\right) g + \mathrm{i}kAh = 0, \tag{93}$$

$$-\left(k^2 D^{(i)} + s\right) h + \mathrm{i}kdRg = 0. \tag{94}$$

The determinant then reads:

$$\left(k^2\Gamma + s^2\rho\right)\left(k^2 D^{(i)} + s\right) + k^2 AdR = 0. \tag{95}$$

To investigate the effect of the coupling, we examine the influence of the various terms. The equation to consider is a cubic polynomial:

$$\rho s^3 + \rho k^2 D^{(i)} s^2 + k^2\Gamma s + k^4 D^{(i)}\Gamma + k^2 AdR = 0. \tag{96}$$

where the values of the prefactors are not known, but their signs can be deducted with the exception of the last term.

Table 1: Values used for the effect of multiphysical coupling on stability.

ρ [kg/m^3]	$D^{(i)}$ [m^2/s]	Γ [Pa]	AdR [Pa/(ms)]
1.0	0.1	-10^{-4}	10^4

An attempt is made herein to visualize the effect of the different terms. For the graphs that follow the values given in table 1 are used unless otherwise stated. In figure 16a the effect of the coupling term on the mechanical problem is illustrated, when the latter is stable. It is clear that positive coupling terms and negative coupling terms with a high absolute value can lead to loss of stability, though the value of s when positive is an increasing function of λ. In fact s is in all cases equal to zero when λ is equal to zero.

For the values given in table 1 the effect of the diffusivity is illustrated in figure 16b. It is clear that the maximum value of s corresponds to a nonzero value of λ, which

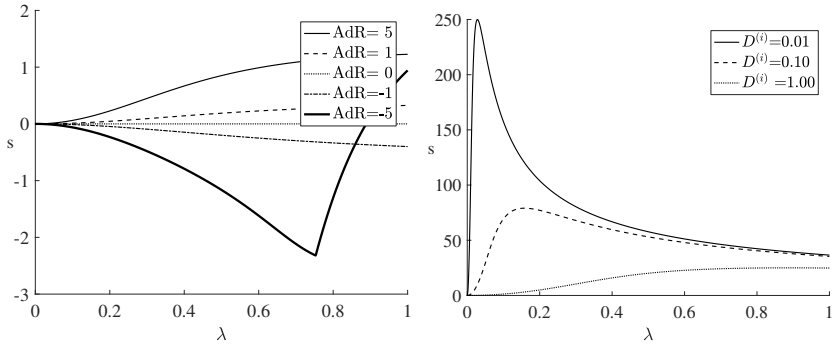

(a) Γ=1.0. (b) Effect of $D^{(i)}$.

Figure 16: s versus λ for different values of parameters.

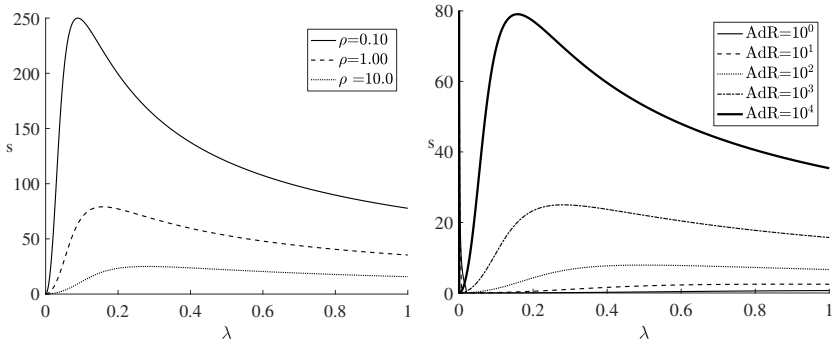

(a) Γ=1.0. (b) $\hat{\Delta}$=0.1.

Figure 17: s versus λ for different values of $\hat{\alpha}$= and $\hat{\Delta}$.

increases with increasing diffusivity, leading one to expect a wider localized zone for higher diffusivity values. On the other hand, changes in the inertia, in the form of changes in the material density, have a very similar effect, changing both the magnitude and location of the maximum value of s, as shown in figure 17a. The effect on the location of the maximum seems to be less pronounced than that of the diffusivity, but this may well be linked to the values selected here.

In figure 17b the effect of the coupling term is illustrated. The most obvious result is an increase in the maximum for increasing values of the coupling term. A detail of this figure is shown in figure 18, illustrating the existence of a first positive branch of s, which goes to infinity for zero λ. This area becomes smaller with increasing values of the coupling term. This results from the mechanical instability and can be

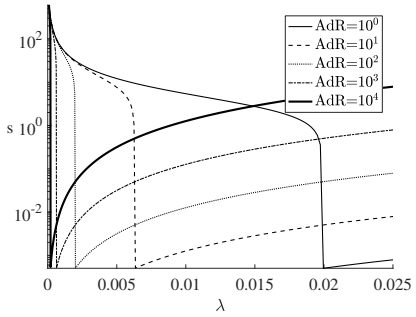

Figure 18: Detail of figure 17b.

alleviated by employing a mechanical response accounting for the materials intrinsic characteristic time or length.

On the whole it may be concluded that (two-way) multiphysical couplings can have both a stabilizing and a destabilizing effect on problem, but in any case introduce a finite width for the localization zone.

5.1 1D Example

The example considered in section 2.5 is revisited here, incorporating thermal coupling. It is assumed that the material exhibits either thermal softening or hardening and that the shearing process generates heat. The constitutive law in its linearized form will read:

$$\begin{aligned} \tilde{\sigma}_{12} &= 2G\frac{h}{1+h}\tilde{\varepsilon}_{12} + A\tilde{T} \\ \tilde{\sigma}_{22} &= M\tilde{\varepsilon}_{22} + B\tilde{T}, \end{aligned} \tag{97}$$

where T stands for the temperature, $M = K + \frac{4G}{3}$ is the p-wave elastic modulus and $h = \frac{1}{G}\frac{d\tau_0}{dq} > -1$ is the hardening modulus.

On the other hand the temperature perturbations have to obey the equation:

$$\frac{\partial \tilde{T}}{\partial t} = \kappa \frac{\partial^2 \tilde{T}}{\partial x^2} + 2\beta\tilde{\varepsilon}_{12}, \tag{98}$$

where κ and β are assumed to be constants.

From the first balance equation and using the usual forms for the perturbations we obtain

$$-(k^2 G\frac{h}{1+h} + s^2\rho)g + \mathrm{i}kA\theta = 0 \Rightarrow \tag{99}$$

$$-(k^2 v_s^2\frac{h}{1+h} + s^2)g + \mathrm{i}k\frac{A}{\rho}\theta = 0. \tag{100}$$

Correspondingly from the heat balance we obtain

$$\mathrm{i}k\beta g - \left(k^2\kappa + s\right)\theta = 0. \tag{101}$$

For more than one non-trivial solutions to exist, the determinant of the system consisting of equations (100) and (101) must be equal to zero:

$$s^3 + k^2\kappa s^2 + k^2 v_s^2 \frac{h}{1+h} s + k^4 v_s^2 \frac{h}{1+h}\kappa + k^2 \frac{A\beta}{\rho} = 0 \Rightarrow \tag{102}$$

$$\hat{s}^3 + \hat{k}^2\hat{s}^2 + \hat{k}^2 \frac{h}{1+h}\hat{s} + \hat{k}^4 \frac{h}{1+h} + \hat{k}^2 \frac{A\beta\kappa}{\rho v_s^4} = 0, \tag{103}$$

with

$$\hat{k} = \frac{\kappa}{v_s} k,\ \hat{s} = \frac{v_s^2}{\kappa} s. \tag{104}$$

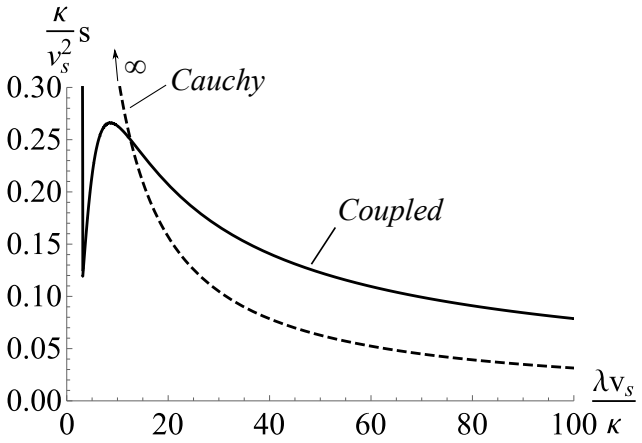

Figure 19: Growth coefficient in function of the perturbation wavelength. While an infinite value is observed for zero wavelength, a second maximum is present.

The growth coefficient as a function of the perturbation length is shown in figure 19. A branch tending to infinity for $\lambda \to 0$ can be observed in a way similar to figure 18. As already mentioned, this is a result of the lack of an internal length or a characteristic time for the material.

6 Conclusions

This chapter focuses on providing the basic tools to graduate students for studying strain localization in solids. The fundamental notions of loss of uniqueness, bifurcation, stability, ill-posedness and mesh dependency are explained through simple examples. Without overlooking classical approaches in bifurcation analysis, we study strain

localization by using the systematic mathematical framework that provides Lyapunov stability. More specifically, we use the first Lyapunov method for exploring the conditions for which equilibria of homogeneous deformation become unstable leading to strain localization. In this method we determine the growth in time of perturbations of arbitrary wavelength from the equilibrium (steady-)state. One-dimensional examples are systematically given to help understanding keeping calculus to the minimum.

First we study strain localization in a classical Cauchy, Boltzmann continuum. We limit our analysis in deformation bands, i.e. compaction, shear, dilation bands and their combinations. This type of strain localization is often observed in several scales, starting from laboratory experiments, such as shear band formation in a granular material or compaction bands in porous rocks, to geological settings, such as faults and landslides. We derive the conditions for strain localization for a general rate-independent constitutive law. Under these assumptions we retrieve the acoustic tensor and we study the dependence of the Lyapunov exponent (growth coefficient) in terms of the perturbation wave length in order to determine the thickness of the localization zone. We show that the perturbations that evolve faster in time (and dominate over the others are characterized by asymptotically zero perturbation wave length and have infinite Lyapunov exponent (singularity in time). This means that deformation bands have zero thickness, which is in contrast with observations. This mathematical artifact explains also the observed mesh-size dependency in finite element analyses of strain localization, when rate-independent Cauchy continua are used.

The aforementioned pathology is partially remedied when rate-dependent Cauchy continua are used. This viscous regularization introduces a characteristic time into the system. Due to the presence of the aforementioned characteristic time, the Lyapunov exponent remains finite (regularization in time). Moreover, when inertia effects are negligible, it renders the system independent of the perturbation wave length. As a result, the behavior of the system during strain localization (e.g. stress-strain profile and deformation band thickness) is determined only by existing imperfections. Such imperfections can be parasitic stresses or material defects. When inertia is not negligible, the dominant perturbation is again the one characterized by the smallest wavelength. Scale analysis shows that inertia terms are important when the perturbation wave lengths are larger than a characteristic wavelength, which depends on the material parameters. Three characteristic times are also identified showing when inertia, viscosity or rate-independent behavior can be neglected. An one-dimensional example using Perzyna viscoplasticity illustrates in a simple way most of the above mathematical findings.

An alternative regularization technique, is the use of Micromorphic continua, such as strain gradient and Cosserat continua, which enrich the continuum description with characteristic lengths. The presence of these lengths remove mesh-size dependency and determine the thickness of the localization zone, which is proportional to the aforementioned internal lengths. Moreover, in the presence of inertia terms the Lyapunov exponent if finite. Therefore, Micromorphic continua remedy both spatial and time singularities, in the expense however of a more complex theory and com-

plicated mathematical derivations. As an example we study strain localization in a rate-independent Cosserat continuum. We use first a general constitutive law in three-dimensions and then we give an one-dimensional example of a sheared infinite layer in order to clarify the mathematical derivations and to illustrate how Cosserat continuum regularizes the problem. Notice, that Cosserat continuum was successfully used by Mühlhauss and Vardoulakis for predicting the shear band thickness of granular materials [MV87].

The chapter closes with a section dedicated to multi-physics couplings and their effects of strain localization. Thermo-Hydro-Chemo-Mechanical effects (THMC, among others) introduce several length and time scales to the system and consequently regularize in a physical manner the underlying mathematical problem. Our analysis is again general, in three-dimensions and considers n-couplings. We show that two-way coupling is necessary for regularization. An one-dimensional example of an infinite layer with thermo-mechanical couplings is then presented for making clear the effects of the various physical mechanism. A rate-independent Cauchy material was used in this last example.

Following this theoretical results and examples the following question is raised:
Which is the best way and theory for best describing strain localization in solids and in particular in geomaterials?
The answer is always found by the modeler and depends on the physical/engineering problem at hand. For instance, for modeling the stress-strain response and the thickness of the principal slip zone of seismic faults (i.e. a narrow shear band formed during seismic slip) a THMC Cosserat continuum was recently used providing realistic predictions [RSS18, RSS18, VSS13]. For studying the damage zone during gallery excavation in the context of radioactive waste disposal a double-scale, poro-mechanical, strain-gradient model was employed [EBC+16].

Acknowledgements

The author, I.S., would like to acknowledge the support of the European Research Council (ERC) under the European Unions Horizon 2020 research and innovation program (Grant agreement no. 757848 CoQuake).

Appendix

A Classical bifurcation analysis and acoustic tensor

Consider a homogeneous, homogeneously deformed solid subjected to quasi-static increments of deformation. Let's assume that after an increment, a deformation band of

thickness H is formed, which breaks the aforementioned homogeneity of the deformation field (and consequently of the stress field) as shown in figure 20. The displacement field remains continuous across the boundaries of the band, but its gradient does not (different strains inside the band):

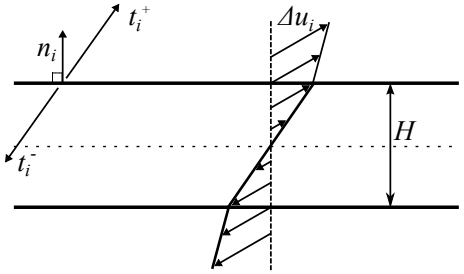

Figure 20: Schematic representation of a deformation band and of the discontinuity of the strain's field.

$$[\![\Delta u_i]\!] = 0 \quad \text{and} \quad [\![\Delta u_{i,j}]\!] = g_i n_j \tag{105}$$

where $[\![.]\!]$ denotes discontinuity across the deformation band boundary (e.g. $[\![\alpha]\!] = \alpha^+ - \alpha^-$), n_i is the orientation vector of the deformation band with $i = 1, 2, 3$ in the three-dimensional space, u_i the displacement field and Δ denotes the increment of a field. $(.)_{,i}$ denotes derivation in terms of x_i.

The jump of the shear stresses at the boundary of the shear band is not zero due to acceleration (not in equilibrium). From the linear momentum balance we obtain:

$$[\![\Delta t_i]\!] = [\![\Delta \sigma_{ij}]\!] n_j = -\rho c [\![\gamma_i]\!] \tag{106}$$

where c is the velocity of a propagating discontinuity in direction n_i such that $[\![\gamma_i]\!] = [\![\Delta v_i]\!] = -c g_i$, with v_i the velocity field (see Hadamard conditions on propagating discontinuities [Had03, LCBD09]). Consider the class of materials that for a small increment Δ, the constitutive law can be written (linearized) as follows:

$$[\![\Delta \sigma_{ij}]\!] = L_{ijkl} \Delta u_{k,l} \tag{107}$$

The tensor L_{ijkl} can be continuous across the boundary of the band ($[\![L_{ijkl}]\!] = 0$) or discontinuous in the sense that elastic unloading can occur outside the band, while continued inelastic loading continues within the band. In the first case we say that we have *continuous bifurcation*, while in the second *discontinuous bifurcation*. It is shown that continuous bifurcation precedes discontinuous bifurcation [RR80]. Inserting Eq.(108) into (106) and using (105) we get:

$$\left(n_j L_{ijkl} n_l - \rho c^2 \delta_{ik}\right) g_k = 0 \tag{108}$$

where $\Gamma_{ij} = n_j L_{ijkl} n_l$ is the acoustic tensor. This equation coincides with equation (8).

References

[AHV+12] Edward Andò, Stephen A. Hall, Gioacchino Viggiani, Jacques Desrues, and Pierre Bésuelle. Grain-scale experimental investigation of localised deformation in sand: A discrete particle tracking approach. *Acta Geotechnica*, 7(1):1–13, 2012.

[Ben05] Ahmed Benallal. On localization modes in coupled thermo-hydro-mechanical problems. *Comptes Rendus Mécanique*, 333(7):557–564, jul 2005.

[BH91a] Davide Bigoni and Tomasz Hueckel. Uniqueness and localization—I. Associative and non-associative elastoplasticity. *International Journal of Solids and Structures*, 28(2):197–213, 1991.

[BH91b] Davide Bigoni and Tomasz Hueckel. Uniqueness and localization—II. Coupled elastoplasticity. *International Journal of Solids and Structures*, 28(2):215–224, jan 1991.

[BN69] F. Brauer and J.A. Nohel. *The Qualitative Theory of Ordinary Differential Equations: An Introduction*. Dover Publications, 1969.

[Bow09] Allan F. Bower. *Applied Mechanics of Solids*. CRC Press, 2009.

[BSS17] Nicolas Brantut, Ioannis Stefanou, and Jean Sulem. Dehydration-induced instabilities at intermediate depths in subduction zones. *Journal of Geophysical Research: Solid Earth*, 122(8):6087–6107, aug 2017.

[BV01] J. P. Bardet and Ioannis Vardoulakis. The asymmetry of stress in granular media. *International Journal of Solids and Structures*, 38(2):353–367, jan 2001.

[CCC06] F. Collin, R. Chambon, and R. Charlier. A finite element method for poro mechanical modelling of geotechnical problems using local second gradient models. *International Journal for Numerical Methods in Engineering*, 65(11):1749–1772, mar 2006.

[CCE98] R. Chambon, D. Caillerie, and N. El Hassan. One-dimensional localisation studied with a second grade model. *European Journal of Mechanics, A/Solids*, 17(4):637–656, 1998.

[CCM01] René Chambon, Denis Caillerie, and Takashi Matsuchima. Plastic continuum with microstructure, local second gradient theories for geomaterials: Localization studies. *International Journal of Solids and Structures*, 38(46-47):8503–8527, 2001.

[CCV04] René Chambon, Denis Caillerie, and Gioacchino Viggiani. Loss of uniqueness and bifurcation vs instability: some remarks. *Revue Française de Génie Civil*, 8(5-6):517–535, 2004.

[DAD+17] Jacques Desrues, A Argilaga, S. Dal Pont, G Combe, Denis Caillerie, and T. kein Nguyen. Restoring Mesh Independency in FEM-DEM Multi-scale Modelling of Strain Localization Using Second Gradient Regularization. In E. Papamichos, P. Papanastasiou, E. Pasternak, and A. Dyskin, editors, *Bifurcation and Degradation of Geomaterials with Engineering Applications. IWBDG 2017. Springer Series in Geomechanics and Geoengineering*, pages 453–457. Springer, Cham, 2017.

[DSMP93] R. De Borst, Lambertus J Sluys, H.B. Mühlhaus, and J. Pamin. Fundamental issues in finite element analyses of localization of deformation. *Engineering Computations*, 10(2):99–121, feb 1993.

[EBC+16] A P Van Den Eijnden, P Bésuelle, F. Collin, René Chambon, and Jacques Desrues. Modeling the strain localization around an underground gallery with a hydro-mechanical double scale model ; effect of anisotropy. *Computers and Geotechnics*, 2016.

[Eri99] A. Cemal Eringen. *Microcontinuum Field Thoeries*. Springer Verlag, 1999.

[Ger73a] P. Germain. La méthode des puissances virtuelles en mécanique des milieux continus - 1. Théorie du second gradient. *Journal de Mecanique Theorique et Appliquee*, 12(2):235–274, 1973.

[Ger73b] P. Germain. The Method of Virtual Power in Continuum Mechanics. Part 2: Microstructure. *SIAM Journal on Applied Mathematics*, 25(3):556–575, nov 1973.

[GSSS16] Michele Godio, Ioannis Stefanou, Karam Sab, and Jean Sulem. Multisurface plasticity for Cosserat materials: Plate element implementation and validation. *International Journal for Numerical Methods in Engineering*, 108(5):456–484, nov 2016.

[Had02] Jacques Hadamard. Sur les problèmes aux dérivées partielles et leur signification physique. *Princeton University Bulletin*, 49-52, 1902.

[Had03] Jacques Hadamard. *Leçcons sur la propagation des ondes et les équations de l'hydrodynamique*. Librairie Scientifique A.Hermann, Paris, 1903.

[IR00] Kathleen A. Issen and John W. Rudnicki. Conditions for compaction bands in porous rock. *Journal of Geophysical Research*, 105(B9):21529, 2000.

[IW98] Maria-Magdalena Iordache and Kaspar J Willam. Localized failure analysis in elastoplastic Cosserat continua. *Computer Methods in Applied Mechanics and Engineering*, 151(3-4):559–586, 1998.

[KABC08] P. Kotronis, S. Al Holo, P. Bésuelle, and R. Chambon. Shear softening and localization: Modelling the evolution of the width of the shear zone. *Acta Geotechnica*, 3(2):85–97, mar 2008.

[LCBD09] Jean Lemaitre, Jean-Louis Chaboche, Ahmed Benallal, and Rodrigue Desmorat. *Mécanique des matériaux solides*. Dunod, Paris, 2009.

[Lya92] Aleksandr Mikhailovich Lyapunov. The general problem of the stability of motion. *International Journal of Control*, 55:531–773, 1992.

[Min64] R.D. Mindlin. Micro-structure in linear elasticity. *Archive for Rational Mechanics and Analysis*, 16(1), 1964.

[Min65] R.D. Mindlin. Second gradient of strain and surface-tension in linear elasticity. *International Journal of Solids and Structures*, 1(4):417–438, nov 1965.

[MV87] Hans-Bernd Mühlhaus and Ioannis Vardoulakis. The thickness of shear bands in granular materials. *Géotechnique*, 37(3):271–283, sep 1987.

[ND11] François Nicot and Félix Darve. Diffuse and localized failure modes: Two competing mechanisms. *International Journal for Numerical and Analytical Methods in Geomechanics*, 35(5):586–601, apr 2011.

[Nee88] A. Needleman. Material rate dependence and mesh sensitivity in localization problems. *Computer Methods in Applied Mechanics and Engineering*, 67(1):69–85, 1988.

[Per66] P. Perzyna. Fundamental problems in viscoplasticity. *Recent Advances in Applied Mechanics*, 9:243–377, 1966.

[PZ16] Panos C. Papanastasiou and Antonios Zervos. Numerical modelling of strain localization. In *Modelling of instabilities and bifurcation in Geomechanics, ALERT geomaterials doctoral school*, 2016.

[RC16] Roozbeh Rezakhani and Gianluca Cusatis. Asymptotic expansion homogenization of discrete fine-scale models with rotational degrees of freedom for the simulation of quasi-brittle materials. *Journal of the Mechanics and Physics of Solids*, 88:320–345, 2016.

[RR75] John W. Rudnicki and James R. Rice. Conditions for the localization of deformation in pressure-sensitive dilatant materials. *Journal of the Mechanics and Physics of Solids*, 23(6):371–394, dec 1975.

[RR80] James R. Rice and John W. Rudnicki. A note on some features of the theory of localization of deformation. *International Journal of Solids and Structures*, 16:597–605, 1980.

[RSS18] Hadrien Rattez, Ioannis Stefanou, and Jean Sulem. The importance of Thermo-Hydro-Mechanical couplings and microstructure to strain localization in 3D continua with application to seismic faults. Part I: Theory and linear stability analysis. *Journal of the Mechanics and Physics of Solids*, 115:54–76, jun 2018.

[SA16] Ioannis Stefanou and S. Alevizos. Fundamentals of bifurcation theory and stability analysis. In Jean Sulem, Ioannis Stefanou, Euripides Papamichos, and Emmanuil Veveakis, editors, *Modelling of instabilities and bifurcation in Geomechanics, ALERT geomaterials Doctoral School 2016*. Aussois, France, 2016.

[SDC07] Giulio Sciarra, Francesco Dell'Isola, and Olivier Coussy. Second gradient poromechanics. *International Journal of Solids and Structures*, 44(20):6607–6629, oct 2007.

[SSV10] Ioannis Stefanou, Jean Sulem, and Ioannis Vardoulakis. Homogenization of interlocking masonry structures using a generalized differential expansion technique. *International Journal of Solids and Structures*, 47(11-12):1522–1536, jun 2010.

[SSV11] Jean Sulem, Ioannis Stefanou, and Emmanuil Veveakis. Stability analysis of undrained adiabatic shearing of a rock layer with Cosserat microstructure. *Granular Matter*, 13(3):261–268, feb 2011.

[Ste18] Ioannis Stefanou. Definition and Uses of the Principle of Virtual Power The Principle of Virtual Power. In *ALERT geomaterials Doctoral School 2018*. 2018.

[SW91] Paul Steinmann and Kaspar J Willam. Localization within the Framework of Micropolar Elasto-Plasticity. *Advances in Continuum Mechanics*, pages 296–313, 1991.

[Var96a] Ioannis Vardoulakis. Deformation of water-saturated sand: I. uniform undrained deformation and shear banding. *Géotechnique*, 46(3):441–456, jan 1996.

[Var96b] Ioannis Vardoulakis. Deformation of water-saturated sand: II. effect of pore water flow and shear banding. *Géotechnique*, 46(3):457–472, jan 1996.

[Var09] Ioannis Vardoulakis. *Lecture notes on Cosserat continuum mechanics with application to the mechanics of granular media*. http://geolab.mechan.ntua.gr/teaching/lectnotes/CCM2009.pdf, 2009.

[VS95] Ioannis Vardoulakis and Jean Sulem. *Bifurcation Analysis in Geomechanics*. Blackie, Glascow, 1995.

[VSS13] Emmanuil Veveakis, Ioannis Stefanou, and Jean Sulem. Failure in shear bands for granular materials: thermo-hydro-chemo-mechanical effects. *Géotechnique Letters*, 3(April-June):31–36, may 2013.

[WSD96] W.M. Wang, Lambertus J Sluys, and René De Borst. Interaction between material length scale and imperfection size for localisation phenomena in viscoplastic media. *European Journal of Mechanics - A/Solids*, 15(3):447–464, 1996.

[ZPV01] Antonios Zervos, Panos C. Papanastasiou, and Ioannis Vardoulakis. A finite element displacement formulation for gradient elastoplasticity. *International Journal for Numerical Methods in Engineering*, 50(6):1369–1388, 2001.